

Synthesis of Submillimeter $\text{SnSe}_x\text{S}_{2-x}$ ($0 < x < 1$) Two-dimensional Alloy and Photoinduced Reversible Transformation between Schottky and Ohmic Contact Behaviors in Devices

Yongtao Li,^a Wenbo Xiao,^b Guangfu Chen,^a Huafeng Dong,^a Xiaoting Wang,^c Tiantian Feng,^a Le Huang,^a Jingbo Li^{*a,c}

a. College of Materials and Energy, Guangdong University of Technology, Guangzhou 510006, People's Republic of China.

b. School of Measuring and Optical Engineering, Nanchang Hangkong University, Nanchang 330063, People's Republic of China.

c. State Key Laboratory of Superlattices and Microstructures, Institute of Semiconductors, Chinese Academy of Sciences, Beijing 100083, People's Republic of China.

**Email - 979139835@qq.com*

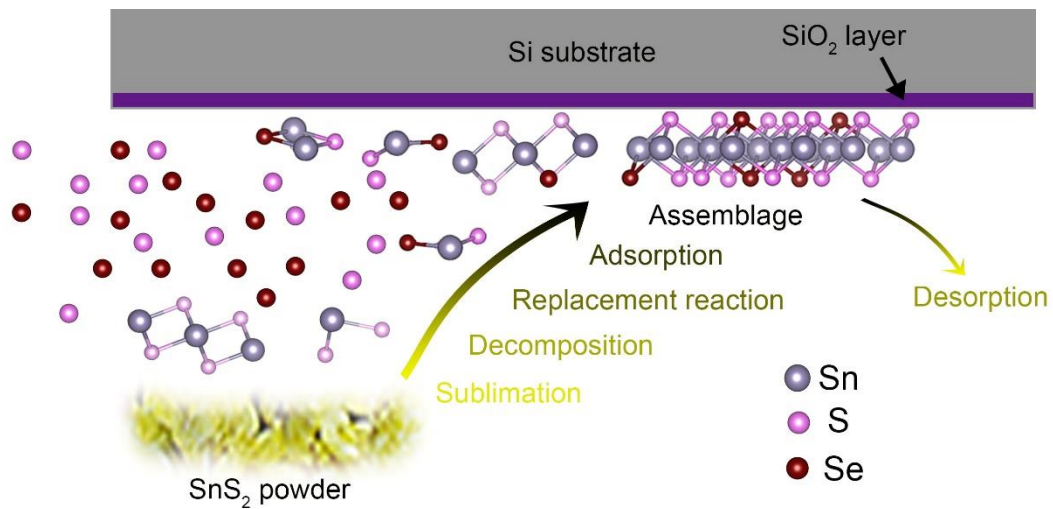


Figure S1. Schematic illustration of the growth process of SnSe_xS_{2-x} alloy, where the SnS₂ powder sublimated and decomposed in the high temperature condition, after which the replacement reaction occurred and some S atoms in the SnS_x molecules were replaced by the Se atoms. Then the intermediate products adsorbed and diffused on the surface of SiO₂/Si substrate and finally assembled into the SnSe_xS_{2-x} FLs.

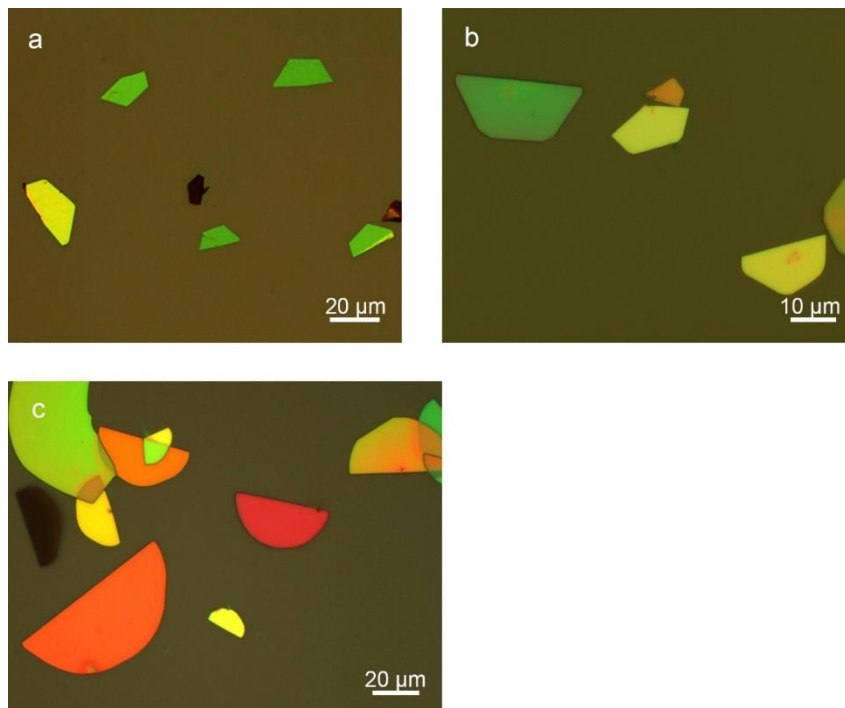


Figure S2. Typical optical images of (a) low Se content ($0 < x < 0.2$), (b) medium Se content ($0.2 < x < 0.6$) and (c) high Se content ($0.6 < x < 1$) $\text{SnSe}_x\text{S}_{2-x}$ flakes on SiO_2/Si substrates.

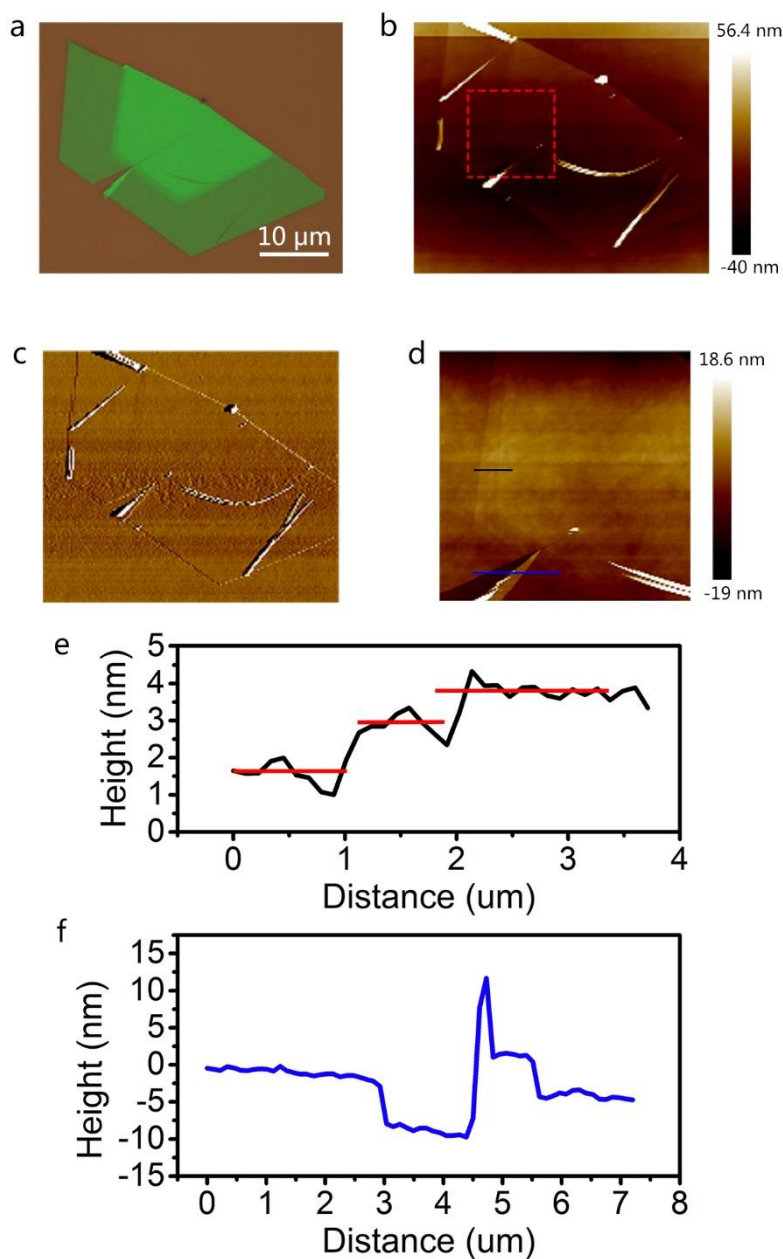


Figure S3. AFM measurement of multilayer semi-hexagonal $\text{SnSe}_x\text{S}_{2-x}$ flake with both cockles and cracks. In our experiment, cockles, rather than cracks, were occasionally seen in the flakes, but they looked like in optical images.

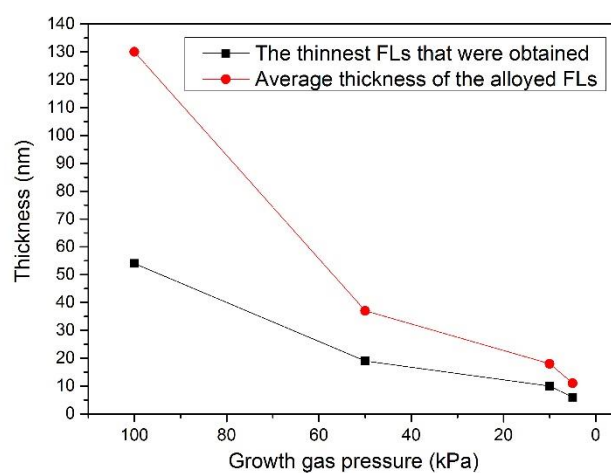


Figure S4. The AFM measured thickness of the $\text{SnSe}_x\text{S}_{2-x}$ FLs that were obtained under different growth gas pressure.

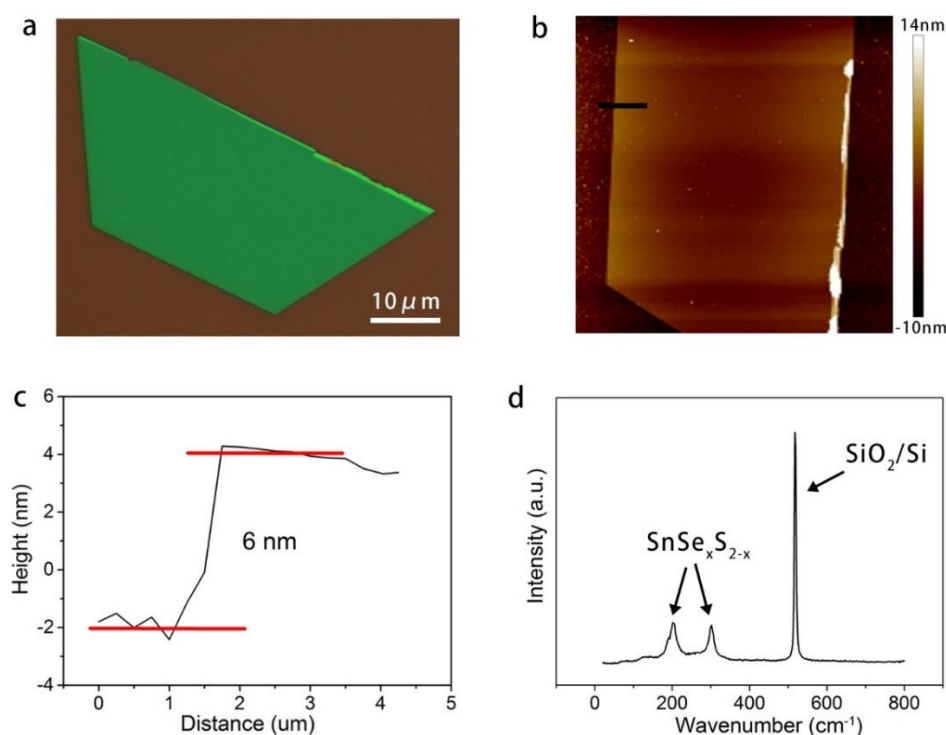


Figure S5. Characterization of LPCVD grown $\text{SnSe}_x\text{S}_{2-x}$ flake on SiO_2/Si substrate. (a) Optical image of semi-hexagonal $\text{SnSe}_x\text{S}_{2-x}$ flake. (b) AFM thickness of the flake in (a). (c) Height profile of the flake. (d) Raman spectrum of the alloyed flake, and peak intensity of the SiO_2/Si substrate was much higher than the peak of $\text{SnSe}_x\text{S}_{2-x}$ flake, revealing that the flake was a thin one.

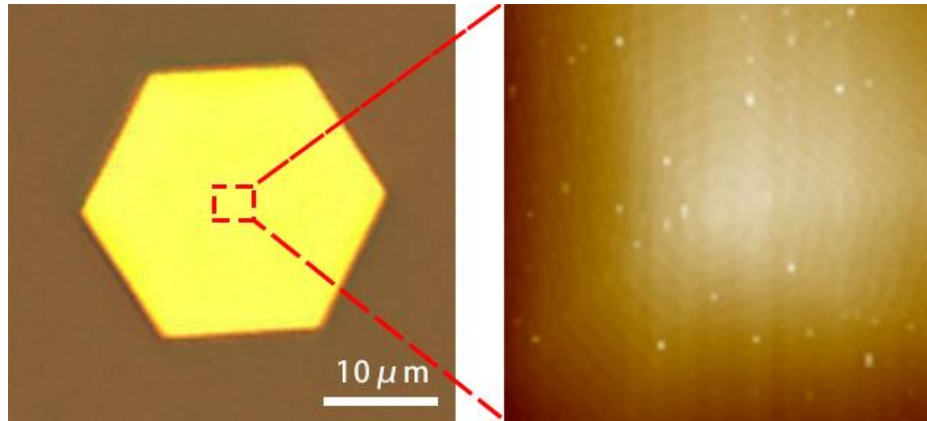


Figure S6. AFM feature of hexagonal flake on SiO₂/Si substrate, presenting an obvious pyramid-like screw structure.

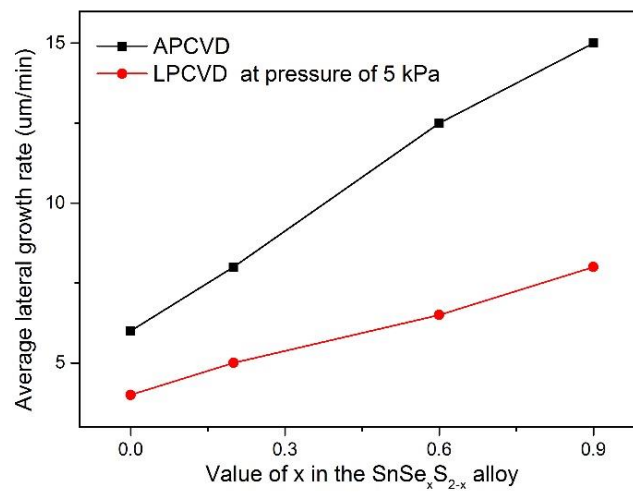


Figure S7. The statistical average lateral growth rate of the SnSe_xS_{2-x} FLs with different value of x under atmospheric pressure and low pressure growth condition. The growth temperature was set as 650 °C.

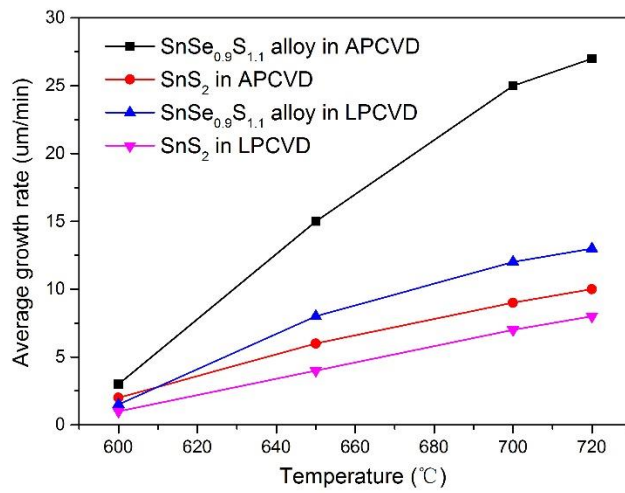


Figure S8. The statistical average lateral growth rate of the SnSe_{0.9}S_{1.1} alloy and pure SnS₂ under different annealing temperature. The gas pressure during LPCVD was wet to be 5 kPa.

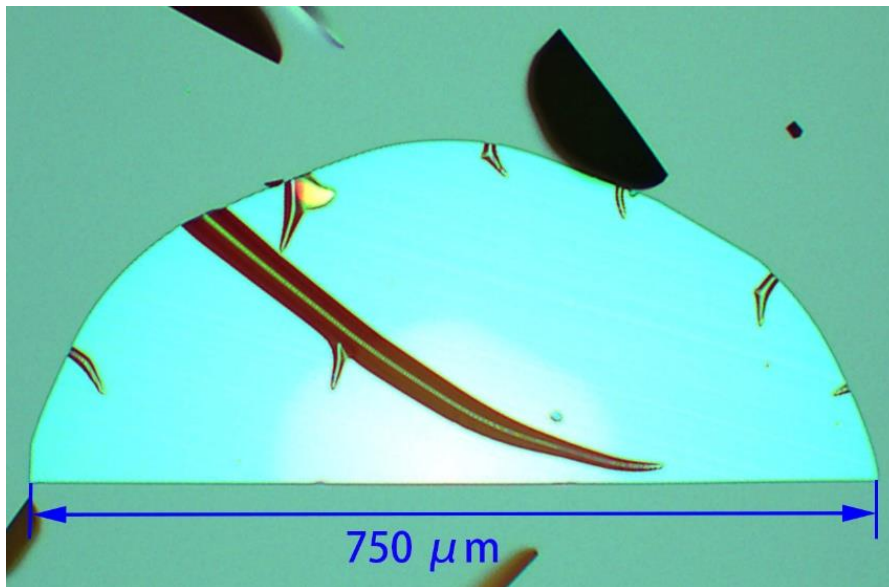


Figure S9. Optical image of the large-area SnSe_xS_{2-x} flake, size of the semi-circle can reach up to 750 μm.

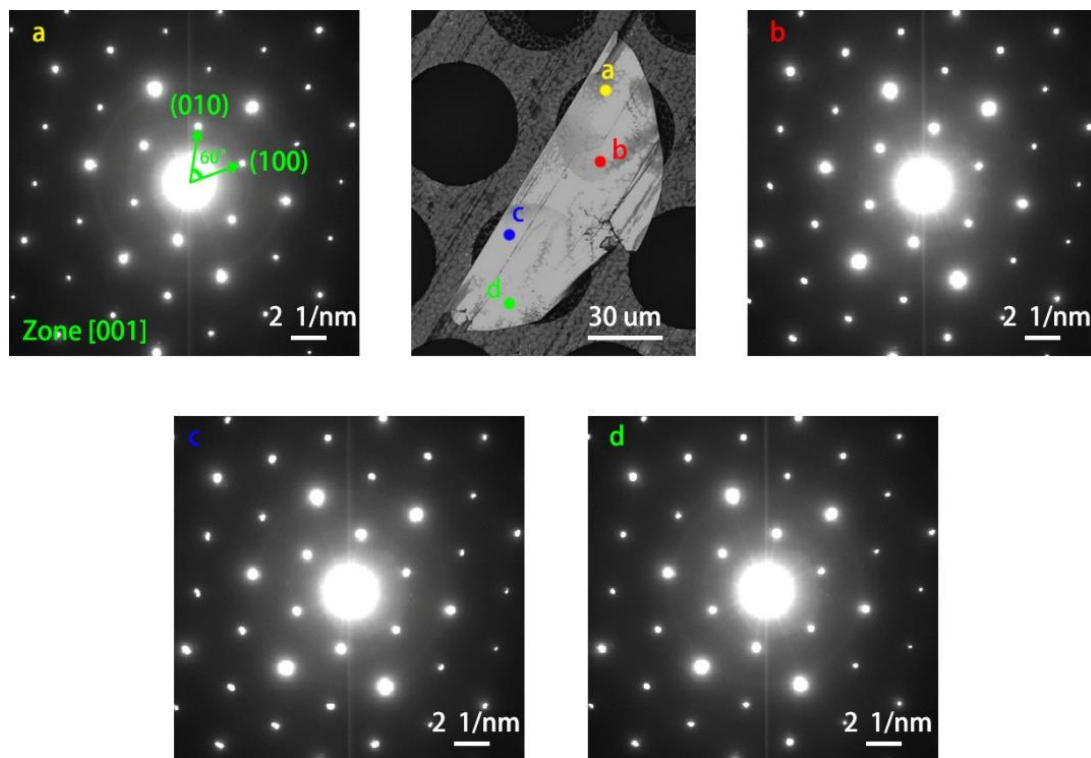


Figure S10. Selected area electron diffraction patterns of the semi-circle $\text{SnSe}_x\text{S}_{2-x}$ flake, different spot of the flake present a consistent orientation, revealing single crystal nature of the sample. And the LPCVD grown semi-hexagonal $\text{SnSe}_x\text{S}_{2-x}$ flake also present a same diffraction pattern.

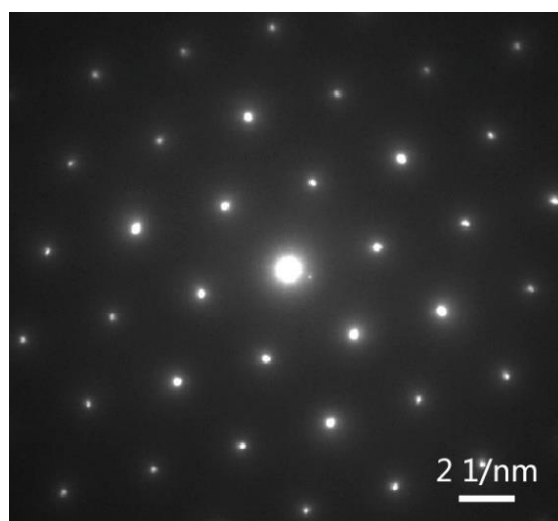


Figure S11. Selected area electron diffraction patterns of the unalloyed SnS_2 flake.

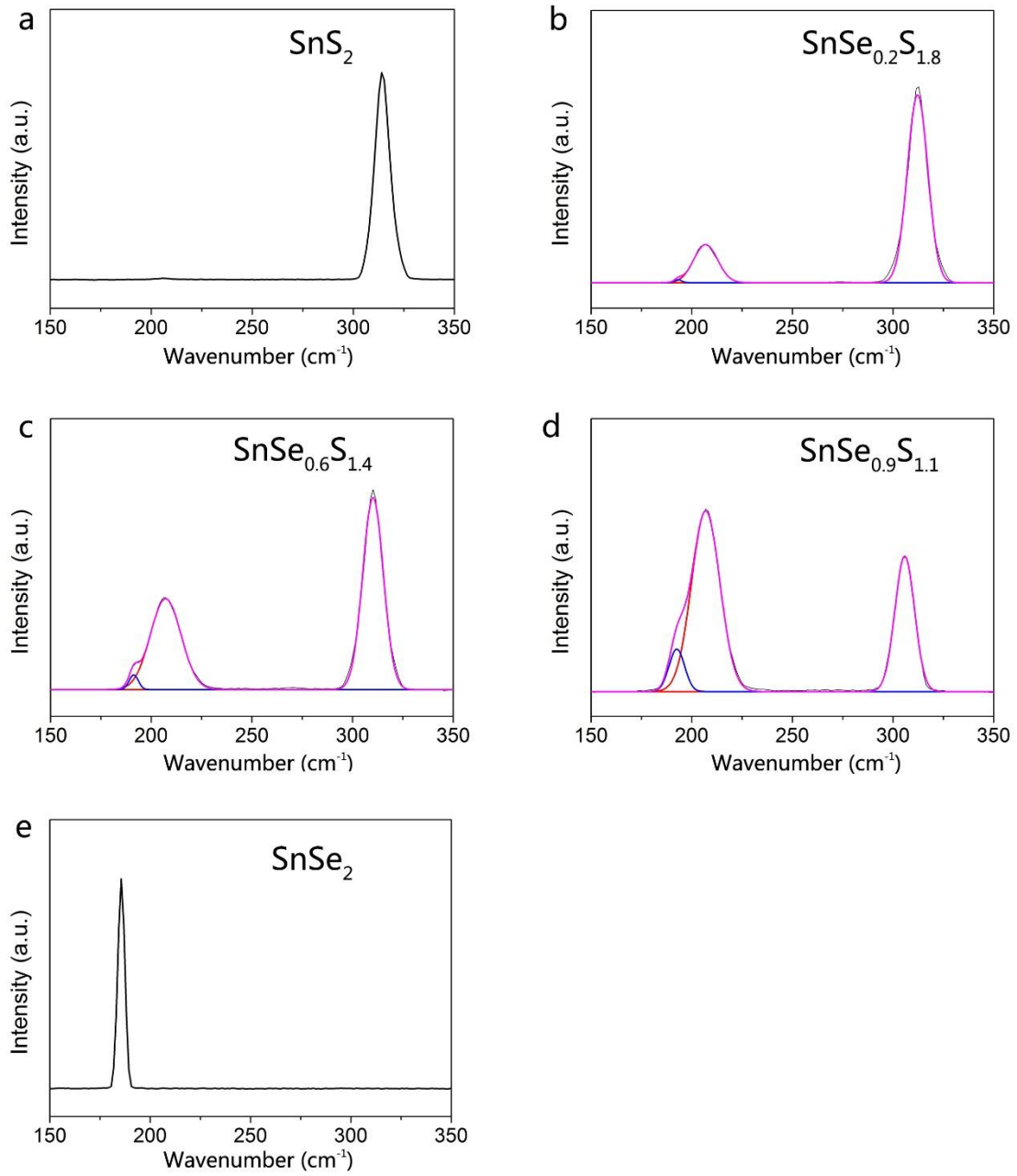


Figure S12. Normalized Raman peaks fitting of (a) SnS_2 , (b) $\text{SnSe}_{0.2}\text{S}_{1.8}$, (c) $\text{SnSe}_{0.6}\text{S}_{1.4}$, (d) $\text{SnSe}_{0.9}\text{S}_{1.1}$ and (e) SnSe_2 , where the left peaks of $\text{SnSe}_x\text{S}_{2-x}$ can be divided into two peaks, respectively.

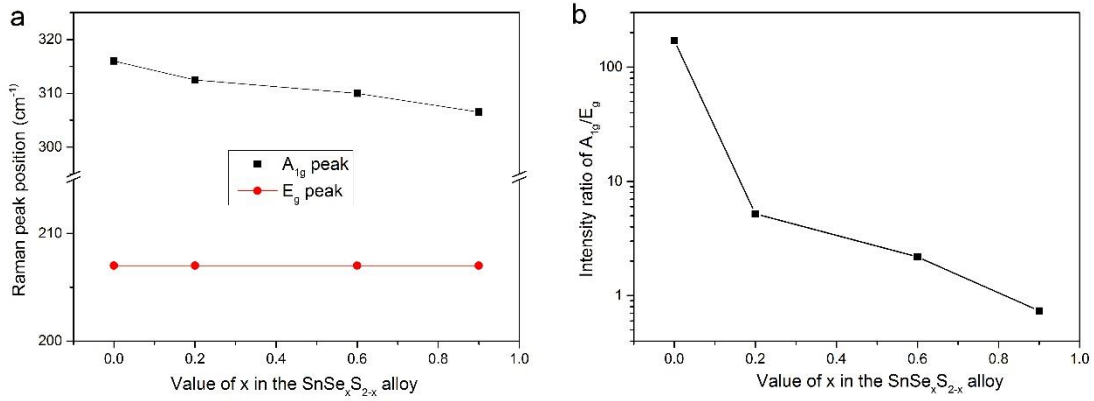


Figure S13. (a) Raman position shift of A_{1g} and E_g peak as function of the value of x in $\text{SnSe}_x\text{S}_{2-x}$, where the A_{1g} peak shift from the 316 cm^{-1} in SnS_2 to the 306.5 cm^{-1} in $\text{SnSe}_{0.9}\text{S}_{1.1}$, while the position of E_g peak remained unchanged. (b) The intensity ratio of A_{1g}/E_g change as function of the value of x in $\text{SnSe}_x\text{S}_{2-x}$ alloy. As the Se content increased, the ratio declined rapidly.

| Material | SnS_2 | $\text{SnSe}_{0.2}\text{S}_{1.8}$ | $\text{SnSe}_{0.6}\text{S}_{1.8}$ | $\text{SnSe}_{0.9}\text{S}_{1.1}$ |
|--|----------------|-----------------------------------|-----------------------------------|-----------------------------------|
| Raman peak position of A_{1g} (cm^{-1}) | 316 | 312.5 | 310 | 306.5 |
| Raman peak position of E_g (cm^{-1}) | 207 | 207 | 207 | 207 |

Table S1. Raman position shift of A_{1g} and E_g peak as function of the value of x in $\text{SnSe}_x\text{S}_{2-x}$.

| Material | SnS_2 | $\text{SnSe}_{0.2}\text{S}_{1.8}$ | $\text{SnSe}_{0.6}\text{S}_{1.8}$ | $\text{SnSe}_{0.9}\text{S}_{1.1}$ |
|---------------------------------|----------------|-----------------------------------|-----------------------------------|-----------------------------------|
| Intensity ratio of A_{1g}/E_g | 170.6 | 5.20 | 2.18 | 0.74 |

Table S2. The intensity ratio of A_{1g}/E_g change as function of the value of x in $\text{SnSe}_x\text{S}_{2-x}$ alloy.

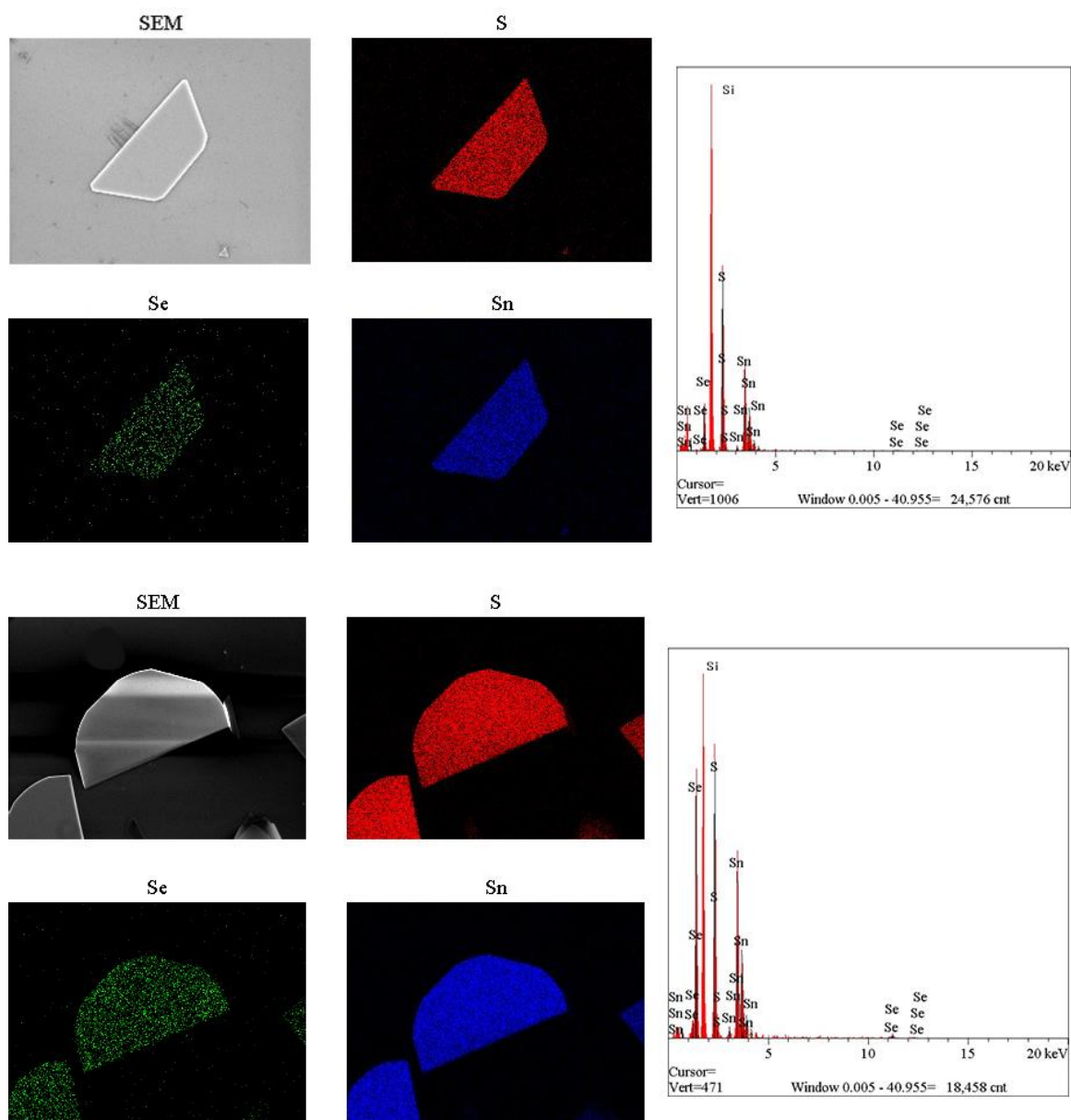


Figure S14. EDX mapping and EDX spectra of medium Se-content ($x=0.5$) and high Se-content ($x=0.9$) $\text{SnSe}_x\text{S}_{2-x}$ alloyed flakes.

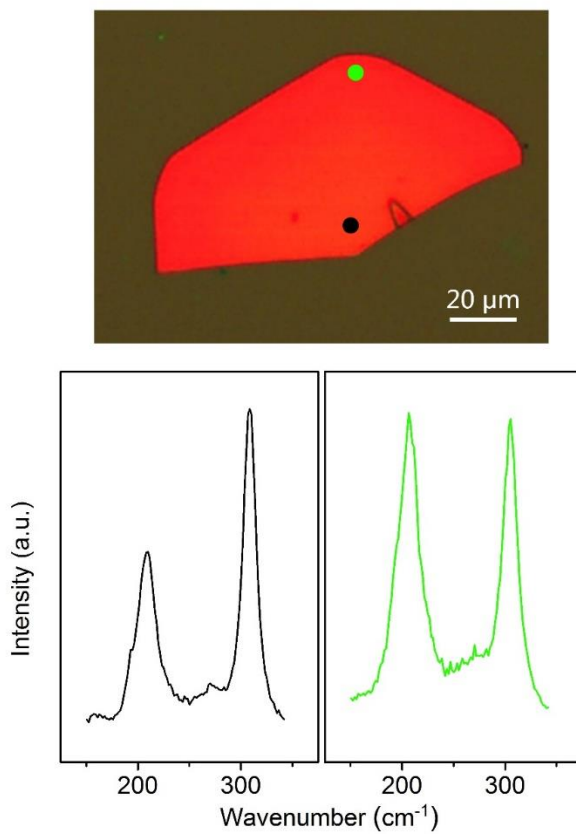


Figure S15. Graded heterostructure with gradual component varying in the $\text{SnSe}_x\text{S}_{2-x}$ single crystal. The raman spectra corrected from different spots indicate obvious compositional variation in the flake, and concentration of Se atoms was gradually increased during the growth process by the mean of pushing the Se boat towards center of the furnace.

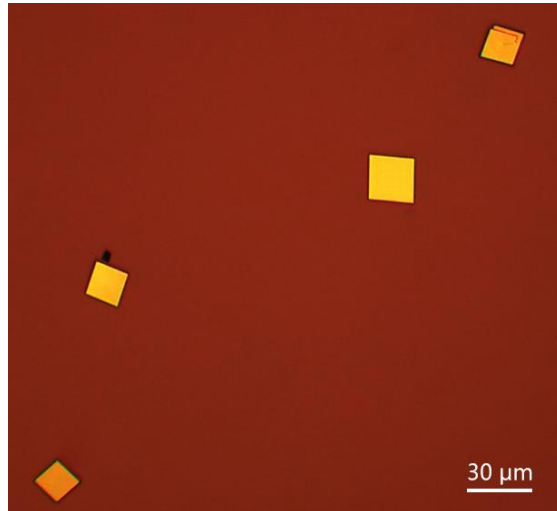


Figure S16. Optical image of square SnS flakes grown on SiO₂/Si substrate. During the synthetic process, SnS₂ powder was used as raw material while no S or Se vapor was introduced into the chamber, the experimental results came out that only SnS, but not SnS₂, flakes could be obtained on the substrate, indicating the fact of decomposition of SnS₂ in high temperature.

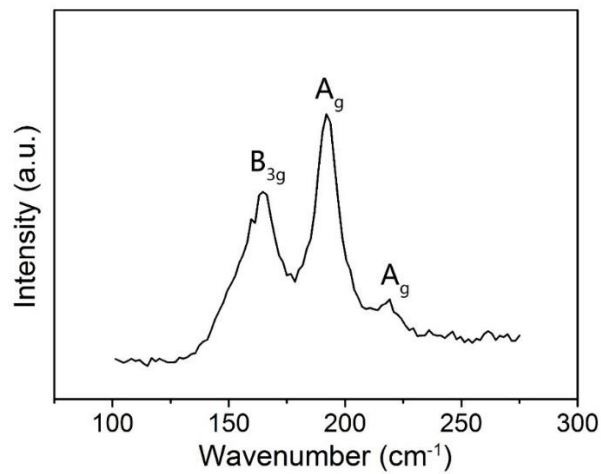


Figure S17. Raman spectrum of the square flakes, the distinct B_{3g} and A_g peak fit well with previous reported SnS flakes, revealing the fact that SnS, rather than SnS₂, flakes were obtained on the substrate when no S or Se vapor was introduced into the furnace.

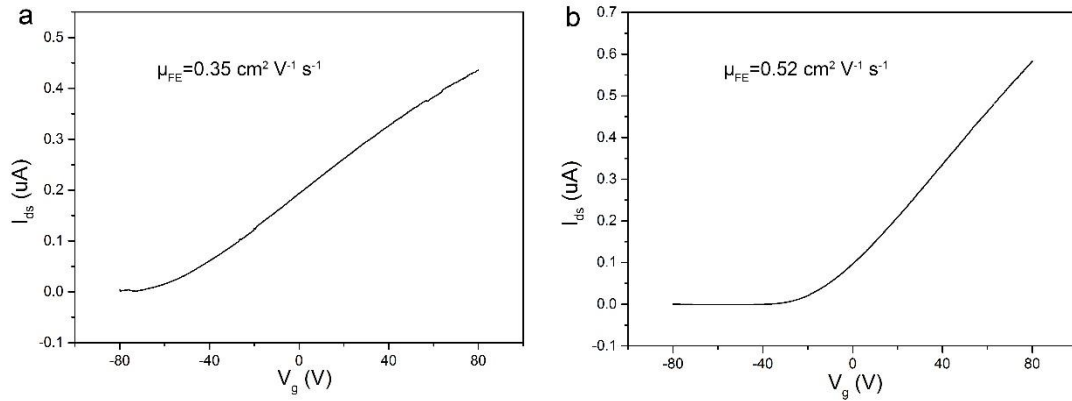


Figure S18. Typical FET device performances comparison based on the CVD grown (a) $\text{SnSe}_{0.9}\text{S}_{1.1}$ and (b) SnS_2 . It could be seen that the threshold voltage of $\text{SnSe}_{0.9}\text{S}_{1.1}$ FET (about -60 V) take a left shift in comparison to the SnS_2 FET (about -20 V). The current on/off ratio of SnS_2 device (about 9600) was also larger than the alloyed one (about 414). The mobility of two devices were close.

| Material | Mobility μ ($\text{cm}^2 \text{V}^{-1} \text{s}^{-1}$) | $I_{\text{light}}/I_{\text{dark}}$ | Rise time (ms) | Fall time (ms) | EQE (%) | Ref. |
|-----------------------------------|---|------------------------------------|-------------------|-------------------|--------------------|----------|
| SnSe_2 | 0.6 | 3 | 14.5 | 8.1 | 2.6×10^5 | 1 |
| SnS_2 | - | 1×10^4 | 22 | 11 | 3.3×10^4 | 2 |
| SnS_2 | - | - | - | 42 | 42 | 3 |
| SnS_2 | 0.001 | 1.5 | 8 | 150 | 115 | 4 |
| $\text{SnSe}_{0.9}\text{S}_{1.1}$ | 0.35 | 21.1 | 0.225 | 0.646 | 1.36×10^3 | Our work |

Table S3. Comparison of electrical properties based on SnS_2 , SnSe_2 and their alloy.

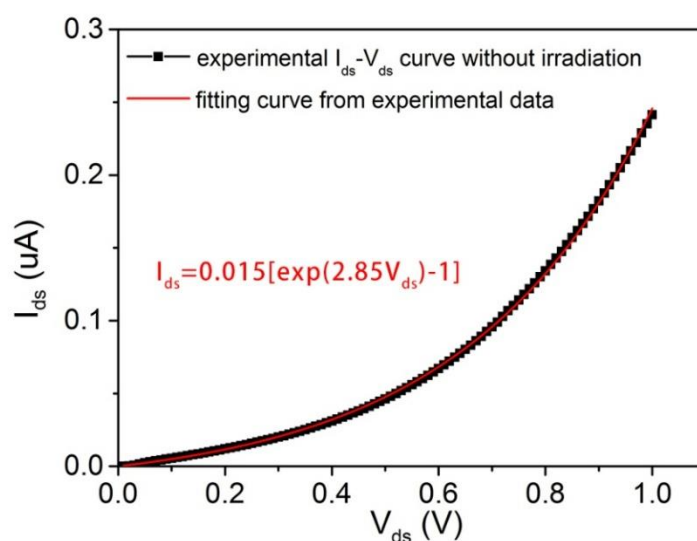


Figure S19. I_{ds} - V_{ds} characteristics of the device under 0 V gate voltage in dark condition, where the fitting curve fitted well with the experimental data, and a function of $I_{ds} = 0.015[\exp(2.85V_{ds}) - 1]$ was extracted from the curve. The exponential increase of I_{ds} as function of V_{ds} indicated SC mode between Au electrode and sample.

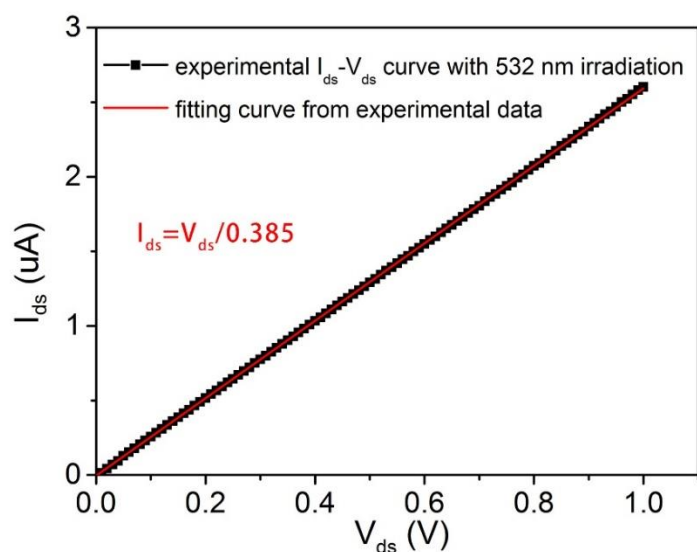


Figure S20. I_{ds} - V_{ds} characteristics of the device under irradiation of 30 mW cm⁻² 532 nm laser without gate effect, where the fitting curve fitted well with the experimental data, and a function of $I_{ds} = V_{ds}/0.385$ was extracted from the curve. The proportional relation between I_{ds} and V_{ds} revealed OC mode between Au electrode and sample

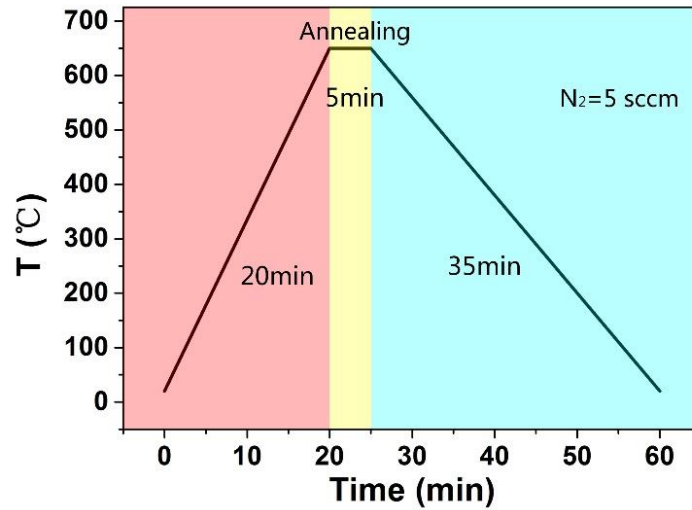


Figure S21. Temperature variation of the furnace during the growth process.

Reference

1. X. Zhou, L. Gan, W. Tian, Q. Zhang, S. Jin, H. Li, Y. Bando, D. Golberg and T. Zhai, *Adv. Mater.*, 2015, **27**, 8035-8041.
2. Y. Huang, H.-X. Deng, K. Xu, Z.-X. Wang, Q.-S. Wang, F.-M. Wang, F. Wang, X.-Y. Zhan, S.-S. Li and J.-W. Luo, *Nanoscale*, 2015, **7**, 14093-14099.
3. J. Xia, D. Zhu, L. Wang, B. Huang, X. Huang and X. M. Meng, *Adv. Funct. Mater.*, 2015, **25**, 4255-4261.
4. G. Ye, Y. Gong, S. Lei, Y. He, B. Li, X. Zhang, Z. Jin, L. Dong, J. Lou and R. Vajtai, *Nano Res.*, 2017, **10**, 2386-2394.